New Materials, Compounds and Applications
Vol.8, No.1, 2024, pp.24-42
https://doi.org/10.62476/nmca8124

COMPUTER SIMULATION OF THE STRUCTURE OF SOME AZO-DERIVATIVES OF β-DIKETONES BY THE METHODS OF QUANTUM CHEMISTRY

S.D. Demukhamedova[1*], I.N. Aliyeva[2]

[1]Department of Biophysics, Institute for Physical Problems, Baku State University, Baku, Azerbaijan
[2]Department of Optics and Molecular Physics, Baku State University, Baku, Azerbaijan

Abstract. The electronic and spatial structures of newly synthesized derivatives of β-diketones were studied based on the results of quantum chemical calculations. The properties of β-diketones with substituted phenyldiazonium chloride, namely 8 tautomers aryl derivatives of β-diketones-(E)-3-(2-(1-(dimethylamino)-1,3-dioxobutan-2-ylidene)hydrazinyl)-2-hydroxy-5-nitrobenzene sulfonic acid (H_3L^1) have been studied using the PM3 semi-empirical quantum chemistry method and the density functional theory (DFT) method with the B3LYP hybrid functional and 6-31+G(d,p) basis set. Energy and electronic characteristics of 8 tautomers are investigated. The effect of intramolecular hydrogen bonding on the structure of the investigated compounds has been studied. The formation of hydrogen bonds was confirmed by Natural Bond Orbital (NBO) analysis. Theoretical studies using the PM3 and DFT methods confirm the practical conclusions about the superiority of the hydrazone form in real samples.

Keywords: *Molecular modeling, spatial and electronic structure, azo-derivatives of β-diketones, hydrogen bonding, quantum chemical calculations.*

Corresponding Author: *Svetlana Demukhamedova, Department of Biophysics, Institute for Physical Problems, Baku, Azerbaijan, Tel.: +99451 526 58 10, e-mail: svetlanabest@mail.ru*

Received: *15 January 2024;* ***Accepted:*** *23 March 2024;* ***Published:*** *15 April 2024.*

1. Introduction

Modern scientific achievements in chemistry, biology and medicine largely depend on the development and implementation of complex mathematical problems that form the basis for the molecular modeling methods. Moreover, computational modeling methods play an important role in the development of new pharmaceuticals. This has become possible due to progress in computer science and significant developments in the field of software, which made it possible to create new computational programs for molecular modeling. Quantum-chemical calculations of polyatomic molecules allow for the obtaining and visual representation of various physical and chemical properties of molecules as well as their geometric, electronic and spectral parameters. Azo derivatives of β-diketones continue to be topical scientific subjects due to their potentially wide range of applications. In particular, materials based on them have been found in wide applications in organic, coordination and supramolecular chemistry and also in medicine;

How to cite (APA):
Demukhamedova, S.D., Aliyeva, I.N. (2024). Computer simulation of the structure of some azo-derivatives of β-diketones by the methods of quantum chemistry. *New Materials, Compounds and Applications, 8*(1), 24-42 https://doi.org/10.62476/nmca8124

the biological significance of arylhydrazones against cancer has been evaluated (Viswanathan *et al.,* 2019). It is known that azo derivatives of *β*-diketones can exist in several tautomeric forms and can rapidly change into each other with proton transfer, accompanied by redistribution of single and multiple bonds. The selection of different substituents can significantly change the physical and chemical properties as well as the biological activity of compounds based on them. Since tautomerism is regarded as a process of proton exchange between two or more forms, it leads to the rearrangement of electron density in tautomers and consequently, to significant changes in the structure and their physical properties and, thus, in their applications. Arylhydrazones of *β*-diketones (AHBD) are well known for their ability to form, depending on the substituents, both O–H…N and N−H…O intramolecular resonant hydrogen bonds (Gilli *et al.,* 2020) accompanied by delocalization of *π*-electrons. Tautomeric balance plays an important role in the application of AHBD as bistate molecular switches (Gilli *et al.,* 2009; Bertolasi *et al.,* 1999; Gilli *et al.*, 2002), ionophores (Kopylovich *et al.,* 2011), antibacterial agents (Shchegol'kov *et al.,* 2010) or selectivity regulators in analytical chemistry (Mahmudov *et al.,* 2008; Mahmudov *et al.*, 2010; Kopylovich *et al.*, 2011; Kuznik *et al.*, 2011). At present, the study of tautomeric effects by various experimental and theoretical methods continues to interest scientists (Udagawa *et al.,* 2021). A review (Hansen, 2021) reviewed the intramolecular interactions of N−H…O, S, N in a wide range of compounds covering many NH donors and hydrogen bond acceptors by spectroscopic methods. Earlier studies are reflected in reviews on tautomeric systems (Martinez *et al.,* 2020; Jezierska *et al.,* 2019) and hydrogen bonding (Hansen, 2016; Hansen, 2017; Sobczyk *et al.,* 2016). At the Centre for Structural Chemistry of the Higher Technical Institute of the University of Lisbon, the synthesis and investigation of various azo derivatives *β*-diketones have been carried out for many years (Kopylovich *et al.,* 2011; Mahmudov *et al.,* 2008; Mahmudov *et al.,* 2010; Kuznik *et al.,* 2011). Studies of azo derivatives of *β*-diketones are continuing (Maspero *et al.,* 2022; Ma *et al.,* 2021; Gurbanov *et al.,* 2020). In our work, eight tautomers synthesized in this laboratory by the reaction between β-diketones and substituted phenyldiazonium chloride-new aryl derivatives of β-diketones-(E)-3-(2-(1-(dimethylamino)-1,3-dioxobutane-2-ylidene)hydrazinyl)- hydroxy-5-nitrobenzene sulfonic acid ($H3L^1$) were studied by the semi-empirical method of quantum chemistry PM3 and DFT method. Since there is no data on NBO analysis of titled structures in the scientific literature, in this work, such a study was carried out for the first time. NBO analysis, which makes it possible to study in detail all the interactions that promote the formation of hydrogen bonds and lead to the stabilization of investigated structures, was carried out. Molecular electrostatic potential (MEP) maps were constructed to accurately the reactivity of the studied compounds.

2. Computational methods

To answer the questions of whether the studied tautomers are planar structures, which of them are the most stable in the gas phase, how the formation of intramolecular hydrogen bonds affects their structure and also to understand the proton transfer process, which is accompanied by a rearrangement of the electron density and consequently, leads to significant changes in structure and physical properties of tautomers, quantum chemical calculations have been carried out. The quantum chemical calculations for predicting the physical and chemical properties of organic molecules are currently considered the most reliable. It is known that by solving the Schrödinger equation, one can obtain all the

properties of the systems under study. To date, the most accurate results can be obtained by solving the Schrödinger equation by ab initio quantum chemistry HF and DFT methods. However, the study of polyatomic molecules by non-empirical quantum chemistry methods requires a large calculation time, which depends mainly on two-electron integrals, which are proportional to the number of basis functions to the fourth power. Therefore, to speed up obtaining the necessary results, it is possible to use semi-empirical methods of quantum chemistry, in which a number of approximations and simplifications are used to solve the Schrödinger equation. All semi-empirical methods are characterized by the fact that the calculation is carried out only for valence electrons, the integrals of certain interactions are neglected, the standard non-optimized basis functions of electron orbitals and some empirical and experimental parameters are used to calculate the values of the integrals (overlapping, Coulomb, exchange, etc.). Experimental parameters eliminate the need to calculate several quantities and correct erroneous approximation results. Part of the interactions is replaced by fitting parameters selected on the basis of a comparison of the calculation of some reference compounds and experimental data. In this case, the solution of the Schrödinger equation is greatly simplified, which leads to high computational efficiency. From the point of view of the approach to solving the molecular Schrödinger equation and the general calculation scheme, semi-empirical and non-empirical methods do not differ. The difference is that due to the use of various approximations, each stage of the calculation is significantly simplified and the calculation speed increases by several orders of magnitude. Since the parametrization of semi-empirical methods is carried out according to the experimental values of certain characteristics of real substances, for some classes of organic compounds, the accuracy of calculating some characteristics of molecules by semi-empirical methods may turn out to be even higher than by ab initio methods (Blatov *et al.*, 2005). Among the semi-empirical methods, the PM3 method is most in demand today, the parameters obtained by comparing a large number and type of experimental data with the results of calculations. Calculated for organic molecules, the PM3 method was also parameterized for other elements, including transition metals. It is known that in calculations by the PM3 method, deviations of bond lengths do not exceed 0.036 Å, bond angles 3-4^0 and the energies of formation of molecules do not exceed 5 kcal/mol.

In this work, we studied the spatial and electronic structure of eight H_3L^1 tautomers with radicals (Figure 1): R_3=OH; R_4=SO_3H; R_5=H; R_6=NO_2; R_1 and R_2 are alternately N$(CH_3)_2$ and CH_3. The calculations were carried out by the semi-empirical quantum-chemical method PM3, using the HyperChem program. Then the obtained results were optimized using the DFT method.

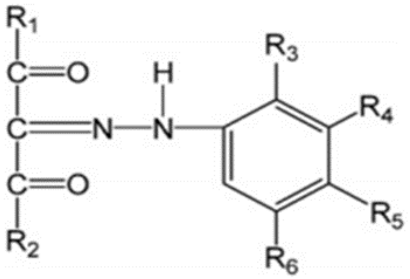

Figure 1. Azo-derivatives of β-diketone

The quantum-chemical study of PM3 was preceded by optimization of the spatial structure of H_3L^1 tautomers within the framework of the MM+ molecular mechanics method using the Polak-Ribiere algorithm until the root mean square gradient reaches 0.001 kcal/mol. The data obtained were used as the basis for the calculation by the semi-empirical PM3 method. Within the framework of this method, the geometrical structure was refined by its optimization by the conjugate gradient method with a step of 0.1 kcal/Å·mol with a different number of iterations until convergence was achieved. The Mulliken model was used to calculate the charge distribution. The effect of different spatial orientation of H_3L^1 tautomeric forms on the geometrical parameters and electron density distribution on atoms of various functional groups has been studied. However, the accuracy of calculation by semi-empirical methods is lower than by *ab initio* methods on an extended basis; the ”non-physicality” of many approximations of semi-empirical methods makes it impossible to predict and explain some properties of the compounds under study. Therefore, to confirm the results obtained, we also carried out calculations at a relatively high level of the electron density functional theory (DFT) with a hybrid three-parameter B3LYP functional and a fairly reliable economical extended two-exponential basis set 6-31+G (d,p) taking into account the polarization functions for all atoms and diffuse functions for non-hydrogen atoms. Due to higher values of the orbital quantum number, polarization functions give the wave function greater flexibility in form, lead to more accurate computed configurations, and help to describe interatomic interactions and chemical bonding well. Diffuse functions have small Gaussian-type orbital s(GTO) exponents. Therefore, they describe the shape of the wave function far from the nucleus and are used to describe interactions at long distances, hydrogen bonds and anions. All calculations were carried out using the Gaussian 09 program (Frisch *et al.*, 2013) and the GaussView 6.0.16 visualizer program (Dennington *et al.*, 2016). As initial data for the calculation of DFT/B3LYP/6-31+G (d,p), the results obtained by the semi-empirical PM3 method were used. We also performed an analysis of the NBO natural bond orbitals (Weinhold *et al.*, 2005) for the obtained optimized structures, the version of the program 3.1 of which was included in the Gaussian 09 software package, which made it possible to obtain detailed information on the electron density delocalization and charge transfer between the interacting atoms of tautomers. In NBO analysis, the input atomic orbital basis set is transformed via natural atomic orbitals (NAOs) and natural hybrid orbitals (NHOs) into natural bond orbitals (NBOs). The NBOs obtained in this fashion correspond to the widely used Lewis picture, in which two-center bonds and lone pairs are localized. A detailed comparison of the *ab initio* DFT calculation with the results of the PM3 calculation was carried out for the lowest energy structure, Hydrazo-III, according to the results of both calculation methods.

3. Results and Discussion

Arylhydrazones of *β*-diketones (HN−N=C=O) are well known for their ability to form intramolecular resonant hydrogen bonds (Gilli *et al.*, 2000). The compounding between the NH donor and the hydrogen bond acceptor is especially important. If it is a double bond or part of an aromatic system, the system was named RAHB (Gilli *et al.*, 2000), which affects the type and strength of the intramolecular hydrogen bond of this type. There is a phenol-azo⇌ hydrazo tautomerism and according to the substituents, O−H…N and N−H…O (RAHB) bonds are formed. In AHBD formed by asymmetric β-diketones, a six-membered H-bonded ring is formed on the more sterically favorable side

of the molecule (Kopylovich *et al.*, 2011). Experiment confirms the formation of a bifurcated (three-centered) H-bond bonding in such systems (Kopylovich *et al.*, 2011). The introduction of an ortho-OH group close to the hydrazone fragment leads to an increase in the number of tautomers. The tautomers studied in the hydrazone forms have a strong RAHB that binds one of the carbonyl groups to the NH-fragment of the hydrazo group of the molecule (Kopylovich *et al.*, 2011).

The paper presents the results of calculations of the spatial and electronic structure of eight tautomeric molecules Z-enol-azo-I, Z-enol-azo-II, E-enol-azo-I, E-enol-azo-II, Keto-azo, Hydrazo-I, Hydrazo-II and Hydrazo-III with the semi-empirical PM3 method of quantum chemistry. The main goal of the study is to determine the tautomers that are most stable in the gas phase, whether their structures are planar, and how the formation of an intramolecular hydrogen bond affects their structure. Figure 2 shows the structures of the investigated tautomers after optimization by the PM3 method, indicating the resulting hydrogen bonds and their lengths. In all tautomers, except Hydrazo forms, the β-diketone fragment is connected by an azo-group $N_{19}=N_{20}$ with an aromatic fragment. In the Hydrazo forms, the azo-group is replaced by a hydrazone group $N_{19}=N_{20}$, and a single N_{20}-C_{21} is replaced by a double bond $N_{20}=C_{21}$. Analysis of the results showed that all tautomers have a quasi-planar structure. The hydroxyl group of the aromatic ring takes a cis-configuration relative to the azo group in the Z-, E-enol-azo and keto-azo tautomers. However, the trans-configuration in Hydrazo-III and II is preferable (deviations are negligible at 15° and 35°, respectively).

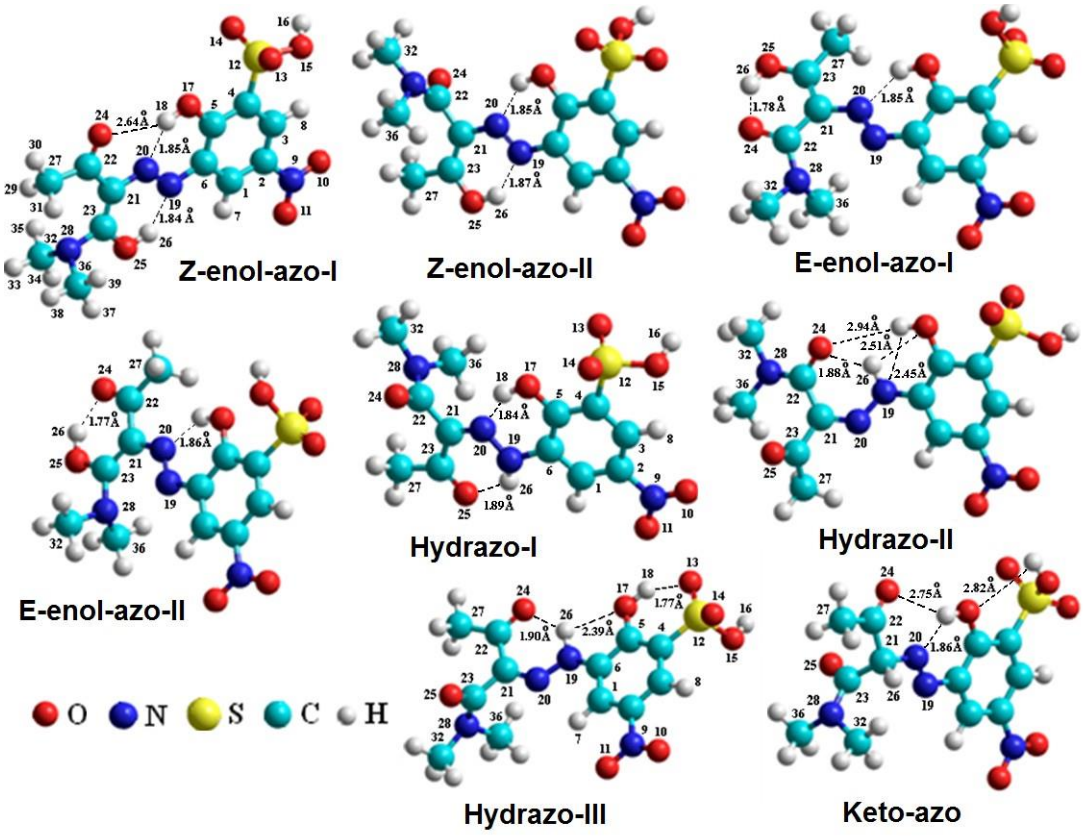

Figure 2. Structures of the investigated molecules calculated by the semi-empirical PM3 method

Table 1 shows the energy parameters, such as values of total electronic energies, relative energy (ΔE) and dipole moments of the tautomers under study. As follows from the results of the calculations, the most stable and compact structure is Hydrazo-III, whose dipole moment (μ) is inferior only to the tautomer E-enol-azo-I, the energy of which is 0.221 eV higher. The Keto-azo tautomer is second in energy, yielding 0.186 eV Hydrazo-III, but its structure is the most expanded (μ = 10.14 D). The other five tautomers have μ=7.00 ÷ 7.62 D. The structure with the highest energy corresponds to the tautomer Z-enol-azo-I, losing to Hydrazo-III only by 0.590 eV.

An analysis of the molecular orbitals is important for calculating the electrostatic potential of a molecule, its donor-acceptor properties (ionization potential, electron affinity) and its excitation potential. The values of energies of the most informative molecular orbitals obtained by calculation are the energy of the higher occupied electron orbital (E_{HOMO}) characterizing the donor properties and energy of the lower vacant orbital (E_{LUMO}) characterizing the acceptor properties of the molecule and their difference ΔE (named GAP energy) are presented in the Table 1. When a molecule is excited, one or more of its electrons transfer from the HOMO to the LUMO one. Accordingly, the first excitation energy of the molecule spent on this transition is equal to $\Delta E = E_{LUMO} - E_{HOMO}$.

Table 1. Energy parameters of the tautomeric forms H_3L^1

Tautomers	Total energy (eV)	ΔE	μ (D)	HOMO (eV)		LUMO (eV)		Δ*E* (eV)	
				α	β	α	β	α	β
Hydrazo-III	-4818.3126	0.0	5.92	-9.402	-9.397	-1.545	-1.508	7.757	7.889
Keto-azo	-4818.1261	0.1865	10.14	-10.269	-10.268	-1.764	-1.810	8.505	8.458
E-enol-azo-I	-4818.0915	0.2212	5.65	-9.694	-9.688	-1.734	-1.725	7.960	7.963
Z-enol-azo-II	-4818.0915	0.2211	7.00	-9.818	-9.814	-1.922	-1.933	7.896	7.881
Hydrazo-I	-4818.0871	0.2255	7.28	-9.691	-9.693	-1.673	-1.665	8.018	8.028
E-enol-azo-II	-4818.0264	0.2862	7.50	-9.916	-9.911	-1.734	-1.745	8.182	8.166
Hydrazo-II	-4817.9179	0.3946	7.59	-9.726	-9.726	-1.479	-1.457	8.247	8.269
Z-enol-azo-I	-4817.7229	0.5898	7.62	-9.967	-9.970	-1.930	-1.924	8.037	8.046

Hardness (η) determines the stability of a compound and is calculated as $\eta=(E_{LUMO}-E_{HOMO})/2$. The higher this value, the more stable the compound. According to Koopmans' theorem, the ionization energy corresponds to negative E_{HOMO} values. The smaller the absolute value, the more reactive the molecule is. We obtained that the Hydrazo-III tautomer is the most and Keto-azo is the least reactive compound. The first perturbation energy has the minimum value for the Hydrazo-III tautomer and the highest value for Hydrazo-II. According to the calculations, the hydrogen bond length varies from 1.77 to 2.94Å. Analysis of the partial charges on the atoms showed that the replacement of the azo group by the hydrazo group leads to a redistribution of charges on the atoms of the benzene ring. A strong hydrogen bond formed between the hydroxyl and sulfo groups

$O_{17}H_{18}…O_{13}$ in Hydrazo-III (1.77Å) and a weaker $O_{15}H_{16}…O_{17}$ in Keto-azo (2.82Å) was observed. In all tautomers except Hydrazo-II and III, stable hydrogen bonds are formed between the hydroxyl group in the ortho-position of the $O_{17}H_{18}$ aromatic ring and the N_{20} nitrogen atom of the azo group (~ 1.85Å). An insignificant 0.01Å increase in the hydrogen bond length in E-enol-azo-II and Keto-azo is associated with an increase in the absolute value of the charge in both tautomers at the N_{19} atom and a decrease at the N_{20} atom. The appearance of a significant positive charge at the N_{19} atom is (0.124) observed in Hydrazo-III, where it participates as a donor in the formation of two hydrogen bonds $N_{19}H_{26}…O_{24}$ (1.90Å) and $N_{19}H_{26}…O_{18}$ (2.39Å). In Hydrazo-I, the charge on the N_{19} atom is 0.111, and hydrogen bond $N_{19}H_{26}…O_{25}$ (1.89Å) is formed. In Hydrazo-II, the charge on the N_{19} atom is 0.032, although H_{26} also forms two H-bonds $N_{19}H_{26}…O_{24}$ (1.88Å) and $N_{19}H_{26}…O_{18}$ (2.51Å), but the N_{19} atom participates as an acceptor in the H-bond $O_{17}H_{18}…N_{19}$ (2.45Å). As can be seen, in Hydrazo-II and III, the hydrogen atom H_{26} of the hydrazo group forms a bifurcated system of two hydrogen bonds with the oxygen atom of the ketone carboxyl group O_{24} (1.88 and 1.90Å) and the oxygen atom O_{17} of the hydroxyl group of the aromatic ring (2.51 and 2.39Å, respectively). In Hydrazo-II, the hydrogen bond $O_{17}H_{18}…N_{19}$ is considerably longer (~ 2.45Å), apparently as a result of the participation of the H_{18} atom in the formation of bifurcated H-bonds - with the N_{19} atom and the carbonyl group $O_{24}C$ (2.94Å). Another hydrogen bond is formed in the Hydrazo-I tautomer between the hydrogen atom of the hydrazine group and the oxygen atom of the ketone carboxyl group (1.89Å). The Hydrazo-II, Z-enol-azo- I and Keto-azo tautomers exhibit H-bond $O_{17}H_{18}...O_{24}$ (2.94, 2.64 and 2.75Å, respectively). Only in Z-enol-azo-I and II hydrogen bonds were formed between the ketone hydroxyl group and the nitrogen atom of the N_{19} azo group (1.84 and 1.87Å). A slight weakening of the hydrogen bond in Z-enol-azo-II due to an increase in its length by 0.03Å is associated with a redistribution of charges on the nitrogen atoms of the $N_{19}=N_{20}$ bonds, as well as changes in the values of valence angles (for example, the angles $C_{23}C_{21}O_{20}$ and $N_{20}N_{19}C_6$ increase by 4.41^0 and 0.81^0 and a decrease in the angles $C_{23}O_{25}H_{26}$, $C_{21}C_{23}O_{25}$ and $N_{19}N_{20}C_{21}$ by 0.90^0, 1.3^0 and 2^0, respectively). Deviation of the torsion angle $C_{23}C_{21}O_{20}H_{26}$ defining the position of the hydroxyl group by 30^0 from the cis position in Z-enol-azo-II was observed. Also, only in E-enol-azo-I and II stable H-bonds are formed in the diketone fragment (1.78 and 1.77Å) between the hydrogen atom of the hydroxyl group $O_{25}H_{26}$ and the oxygen atom of the carboxyl group of ketone $C_{22}=O_{24}$. A slight decrease in the hydrogen bond length by 0.01Å is associated with insignificant redistribution of charges on the CO and OH groups of these tautomers.

The formation of H-bonds is accompanied by changes in the geometric parameters of the compounds. In the sulfo group, the C-S bond length in all tautomers has a value 1.8Å and decreases by 0.03Å only in Keto-azo. The hydroxyl group, $O_{17}H_{18}$, is characterized by C-O lengths of ~ 1.34Å and O_{17}-H_{18} of~ 0.97Å, which increases and decreases only in Hydrazo-II by 0.02Å, respectively. The C_6-N_{19} bond length is 1.44Å in all tautomers except the Hydrazo forms, in which it increases by 0.01Å. The N=N bonds have a length of 1.24Å in the Z- and E-enol-azo tautomers and 1.23Å in the Keto-azo. In Hydrazo-I, II and III tautomers, the N_{19}-N_{20} bond is single with lengths of 1.36, 1.37 and 1.35Å, respectively. In Hydrazo-forms, the double bond $N_{20}=C_{21}$~ 1.31Å; in other tautomers, the N_{20}-C_{21} bond is single and has a value~ of 1.43Å, increasing by 0.06Å in Keto-azo. The longest C_{21}-C_{22} bond length of 1.54Å is observed in Keto-azo, but in the tautomers Z-enol-azo and Hydrazo-I and II, it is 1.5 Å, in E-enol-azo and Hydrazo-III ~ 1.49Å. The double bond C_{21} =C_{23} in Z- and E-enol-azo is equal to 1.38 Å and the single

bond C_{22}-C_{23} in Hydrazo tautomers is 1.5Å and in Keto-azo 1.54Å. The C_{22}=O_{24} bond length varies within 1.22 ÷ 1.24Å regardless of whether the CH3 or N $(CH_3)_2$ group is nearby.

Analysis of the valence angles shows that in the sulfo group, the C-S=O angles are ~110^0 ÷ 111^0, but in the Hydrazo-III tautomer, where the H-bond is formed, one of them decreases to 106.9^0 and the other increases to 113.3^0. The position of the hydroxyl group $O_{17}H_{18}$ determined by the $O_{17}C_5C_6$ angle having the value ~ 123^0 and only in the Hydrazo-III tautomer is 115.9^0. In Hydrazo-forms, the N-N bond is single; the $C_6N_{19}H_{26}$ and $N_{20}N_{19}H_{26}$ angle values vary between 112 ÷ 118^0, the lowest value observed in Hydrazo-III (113.9 and 112.6^0). The angle of $C_6N_{19}N_{20}$ is also minimal in Hydrazo forms (115.9^0 in Hydrazo-II, 116.4^0 in Hydrazo-I and 116.9^0 in Hydrazo-III), in other tautomers this angle is 118^0. In Hydrazo forms, the valence angle of $N_{19}N_{20}C_{21}$ also increases (~ 123^0). In the Z- and E-enol-azo tautomers, the $N_{20}C_{21}C_{22}$ angles are ~ 111 ÷ 115^0 and $N_{20}C_{21}$=C_{23}~ 122 ÷ 126^0. In the Keto-azo tautomer, these angles take on values 109.1^0 and 112.3^0 (because the C_{21} atom participated in the formation of another $C_{21}H$ bond). In Hydrazo-I and III, the angles N_{20}=$C_{21}C_{22}$ and N_{20}=$C_{21}C_{23}$~ 116^0 and 124^0, respectively and in Hydrazo-II, their values change and have a value of 122^0 and 115^0. All values of the C−C=O angles lie in the range ~ 120 ÷ 122^0, and the C−C−O angles lie in the range 123 ÷ 126^0. The $C_{23}O_{25}H_{26}$ angle in Z- and E-enol-azo has a value of ~ 111^0. The $C_6N_{19}N_{20}C_{21}$ dihedral angle in the Hydrazo forms decreases by 16^0 in Hydrazo-III, 18^0 in Hydrazo-I and 21^0 in Hydrazo-II as compared to other tautomers where it is trans-configured.

Due to electron density delocalization, replacing the azo group with a hydrazo group leads to a redistribution of charges on the atoms. Atoms of the hydroxyl group O_{17} and H_{18} in Hydrazo-II showed the lowest negative (−0.214) and positive (0.230) charges for all tautomers studied and the highest negative (−0.256) and positive (0.281) charges in Hydrazo-III, respectively. The N_{19} atom in the E-enol-azo-II tautomer, which is not involved in the formation of the hydrogen bond, has an increased charge compared to the other Z- and E-enol azo tautomers and becomes positive. In Hydrazo forms, a hydrogen atom appears at the N_{19} atom, so increasing (0.111, 0.084, 0.124) and decreasing (−0.029, −0.014, −0.013) in charge at the N_{20} atom were observed. The Keto-azo has an even more negative charge (−0.081) on the N_{20} atom since, due to the CH bond, atom C_{21} exhibits the largest negative charge (−0.132). In the E-enol-azo-II tautomer, the N_{19} atom is not involved in forming the hydrogen bond, so its charge increases and becomes positive. In Hydrazo-III, the PM3 optimization results lead to the formation of a strong hydrogen bond $O_{17}H_{18}$...O_{13} between the hydroxyl and sulfo groups and redistribution of the sulfo group charges (O_{13} has the largest negative charge (−0.896), O_{14} has the smallest (−0.810). At the C_{21} atom, the negative charge in Z- and E-enol-azo takes values in the range −0.335 ÷ −0.377, decreases in Hydrazo (−0.242 ÷ −0.278) and Keto-azo (-0.132). The C_{22} and C_{23} atoms have a positive charge (0.37 ÷ 0.22) and the C_{27} atom is negative (−0.107 ÷ −0.165). In Keto-azo, the charge on the O_{24} atom increases (−0.278).

An analysis of the orbital occupancy ratios of atoms makes it possible to study changes in electron density distribution both by displacements (the numerical value of the occupancy of a given orbital by electrons) and by directions (values of occupancy ratios decomposed along coordinate axes). Let us analyze the population of the atoms participating in the formation of hydrogen bonds of the most stable tautomer, Hydrazo-III. The p_z orbitals of oxygen O_{13} and O_{17} atoms (~ 0.9) and nitrogen N_{19} (~ 0.76) and p_y (0.81) and p_z (0.75) orbitals of O_{24} turn out to be the most electron-populated.

Optimization reduces the electron occupancy of the constituent alpha and beta orbitals by 0.013 (the p_y orbital of the O_{13} atom) and by 0.018 (the p_z orbital of the O_{17} atom). In the alpha orbital of the oxygen atom O_{24}, the occupancy decreases by 0.012 on the p_y orbital. It increases by 0.014 on the p_z orbital, while the beta orbital decreases in the p_y and p_z orbitals population by 0.014 and 0.011, respectively. In the hydrogen atoms H_{18} and H_{26}, the occupancy of the s-orbitals decreases by 0.005 in both orbitals (alpha and beta) of the H_{18} atom and increases in the H_{26} atom (by 0.003 and 0.004 in the alpha and beta orbitals, respectively).

The analysis of the charge distribution on the atoms and orbital occupancies for the Hydrazo-III tautomer showed that the negative charge on the O_{24} atom (−0.349) is larger than on the O_{17} atom (−0.256); therefore, the probability of hydrogen bonding with the H_{26} atom is larger for this atom. H_{18} interacts with atom O_{13}(−0.896) of the sulfo group and forms an H-bond with a length of 1.77Å, pulling away the hydroxyl group from the H_{26} atom. This situation leads to the weakening of H-bond $N_{19}H_{26}...O_{17}$ (2.39Å) and to the formation of stable RAHB $O_{24}...H_{26}$ (1.90Å) with electrons delocalization along the atomic ring. Thus, based on the analysis of changes in the electron density, charge values, total energies, dipole moment values, and HOMO and LUMO contributions, we theoretically characterized the stable structures of the studied tautomers obtained after quantum-chemical calculations using the PM3 method.

After a detailed analysis of the calculation results obtained by the PM3 method, the calculations by the DFT method with the B3LYP hybrid functional, which are most suitable today for such studies, were carried out. The well-established 6-31+G(d,p) basis set supplemented with diffuse functions for non-hydrogen atoms and polarization functions for all atoms was chosen as the basis set. As a result of the calculation performed by the DFT/B3LYP/6-31+G(d,p) method, the geometric, energy and electronic parameters of the tautomers were obtained and analyzed (Table 2).

Table 2. Energy parameters of the tautomeric forms of H_3L^1 according to the calculation data by the method DFT/B3LY P/6-31+ G(d, p)

Tautomers	Energy (eV)	μ (D)	HOMO (eV)	LUMO (eV)	GAP (eV)
Hydrazo-III	-45839.947501	5.0855	-6.736182	-3.194346	3.541836
Hydrazo-I	-45839.736759	6.7481	-6.952785	-3.292579	3.660206
E-enol-azo-II	-45839.642537	10.4463	-6.795503	-3.163869	3.631634
E-enol-azo-I	-45839.612495	6.4886	-6.864075	-3.204142	3.659933
Z-enol-azo-II	-45839.582947	6.2660	-6.960948	-3.587551	3.373397
Hydrazo-II	-45839.490264	6.0374	-6.990336	-3.216659	3.773677
Keto-azo	-45839.348441	10.9293	-7.747085	-3.624830	4.122255
Z-enol-azo-I	-45839.163989	11.7960	-6.584614	-3.061554	3.523060

Table 2 includes values of the electronic energy, the energies of the boundary HOMO and LUMO orbitals, their energy gap and dipole moments. The lower vacant orbital (LUMO) energy sign determines whether a molecule belongs to electrophilic or nucleophilic reagents. The negative sign of the energy of the LUMO orbital for all the studied tautomers indicates their electrophilicity. Analyzing the energies of frontier orbitals, one can obtain a large amount of information about the chemical properties of molecules. According to the Koopmans theorem (1934), the first ionization energy of a molecular system is equal to the negative value of the HOMO orbital: $I = -E_{HOMO}$. Electron affinity is defined as the negative value of the LUMO orbital: $A = -E_{LUMO}$.

Comparing the results of PM3 (Table 1) and DFT (Table 2) calculations showed the change in the sequence of tautomers according to the value of the total electronic energy. Keto-azo tautomer from the second position (according to PM3) moved to the seventh position (according to DFT), which is quite reasonable and corresponds to the data of other calculations of similar tautomers (Mahmudov *et al*., 2013). However, the most stable tautomer according to the calculation data by PM3 of the Hydrazo-III, as well as the result of the calculation by the DFT/B3LYP/6-31+G(d,p) method, also turned out to be the lowest energy and most compact in configuration, its dipole moment has the smallest value (5.08 D). The second tautomer, Hydrazo-I, loses 0.21 eV in comparison to the lowest energy structure of Hydrazo-III. In the present work, we compared the results obtained for the lowest energy structure, Hydrazo-III (according to the results of calculations by the PM3 and DFT methods). Figure 3 shows the DFT/B3LYP/6-31+G(d,p) optimized structures of the Hydrazo-III tautomer.

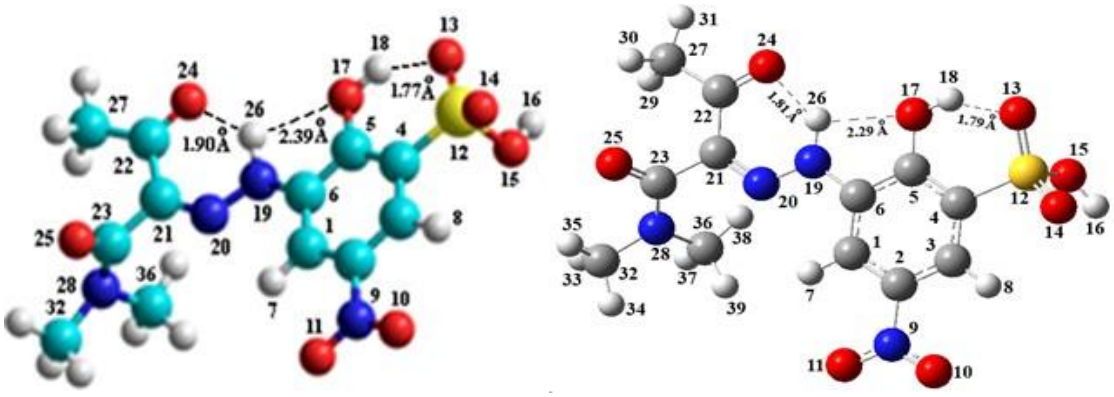

Figure 3. Hydrazo-III structure obtained by PM3 optimization (on left) and DFT/B3LYP/6-31+G(d,p) calculations (on right)

Table 3 shows the selected geometric parameters of the bond lengths, bond and dihedral angles of the Hydrazo-III tautomer for the rings formed by hydrogen bonds due to non-valent interactions. In the first line of each ring, the length of the corresponding hydrogen bond and the bond angle confirming its formation are shown.

DFT optimization led to an increase in the resonant hydrogen bond $N_{19}H_{26}…O_{24}$, which shortened by 0.085Å and became equal to 1.81Å. In this case, there is no significant change in the geometric parameters of the resonant ring. As follows from Table 3, the largest change in bond lengths is associated with an increase of 0.012Å in the length of $N_{19}H_{26}$ and $C_{22}O_{24}$ and decreasing of 0.029Å in the length of $N_{20}N_{19}$ in the case of RAHB. In this case, the valence angle $N_{20}N_{19}H_{26}$ increased by about 4.21⁰, while angles $C_{21}N_{20}N_{19}$ and $O_{24}C_{22}C_{21}$ decreased by 1.617⁰ and 0.263⁰, respectively. The $C_6N_{19}N_{20}C_{21}$ dihedral angle changing by 14^0 corresponds to a purely trans-arrangement, and the angle $N_{19}N_{20}C_{21}C_{22}$ changing by 11^0 corresponds to a purely cis-arrangement. The formation of a resonant hydrogen bond is confirmed by NBO analysis. Another strong hydrogen bond, $O_{17}H_{18}…O_{13}$, lengthens by 0.014Å only, although DFT optimization increases the bond lengths of this resulting ring by a maximum of 0.01^0 (C_4S_{12} and $O_{17}H_{18}$ bond lengths).

Table 3. Geometrical parameters Hydrazo-III according to the results of PM3 and DFT/B3LYP /6-31+G(d,p) calculations

Bond lengths (Å)			Bond angles (degree)			Dihedral angles (degree)		
Atoms	PM3	DFT		PM3	DFT		PM3	DFT
RAHB								
$N_{19}H_{26}\ldots O_{24}$	1.89937	1.81393	$N_{19}H_{26}\ldots O_{24}$	128.897	130.09598			
$N_{19}N_{20}$	1.35480	1.32544	$O_{24}C_{22}C_{21}$	119.653	119.38984	$C_6N_{19}N_{20}C_{21}$	164.268	178.258
$N_{20}C_{21}$	1.31352	1.30781	$C_{22}C_{21}N_{20}$	124.642	124.65691	$N_{19}N_{20}C_{21}C_{22}$	-9.358	1.266
$C_{21}C_{22}$	1.49237	1.48990	$C_{21}N_{20}N_{19}$	122.820	121.20229	$N_{20}C_{21}C_{22}O_{24}$	3.041	-0.060
$C_{22}O_{24}$	1.22533	1.23737	$N_{20}N_{19}H_{26}$	114.497	118.70655	$H_{26}N_{19}N_{20}C_{21}$	21.005	0.059
$N_{19}H_{26}$	1.01487	1.02656				$N_{19}N_{20}C_{21}C_{23}$	177.051	-
Structure with sulfo group SO_3H								
$O_{17}H_{18}\ldots O_{13}$	1.77742	1.79099	$O_{17}H_{18}\ldots O_{13}$	148.126	147.25191			
C_4C_5	1.41404	1.40991	$O_{17}C_5C_4$	123.774	125.54682	$C_5C_4S_{12}O_{13}$	4.055	20.371
C_4S_{12}	1.76872	1.78152	$C_5O_{17}H_{18}$	111.023	110.38613	$C_4C_5O_{17}H_{18}$	-1.825	-8.052
$S_{12}O_{13}$	1.46415	1.46800	$C_5C_4S_{12}$	123.127	120.34361			
C_5O_{17}	1.34593	1.34100	$C_4S_{12}O_{13}$	106.855	107.20457			
$O_{17}H_{18}$	0.96747	0.98254						
Structure with hydroxyl group OH								
$N_{19}H_{26}\ldots O_{17}$	2.39593	2.29246	$N_{19}H_{26}\ldots O_{17}$	97.3836	98.06110			
C_6N_{19}	1.44944	1.39180	$H_{26}N_{19}C_6$	117.561	121.58608	$C_5C_6N_{19}N_{20}$	-165.00	179.980
$N_{19}H_{26}$	1.01487	1.02656	$N_{19}C_6C_5$	118.898	116.88623	$N_{19}C_6C_5O_{17}$	5.283	0.075
C_6C_5	1.42796	1.42118	$C_6C_5O_{17}$	115.905	116.05866	$C_5C_6N_{19}H_{26}$	-22.876	-1.874
C_5O_{17}	1.34593	1.34100						

The maximum change in bond angles corresponds to a decrease in the $C_5C_4S_{12}$ angle by 2.78^0 and an increase in the $O_{17}C_5C_4$ angle by 1.77^0. The length of the weak hydrogen bond $N_{19}H_{26}\ldots O_{17}$ decreases by 0.1Å and becomes equal to 1.29Å. The bond angle of $H_{26}N_{19}C_6$ is reduced by 4^0, and the angle of $N_{19}C_6C_5$ is reduced by 2^0. The dihedral angle of $C_5C_6N_{19}N_{20}$ increases by 15^0 and corresponds to the purely cis-configuration.

Table 4 lists the Mulliken charges for the Hydrazo-III tautomer calculated by the PM3 and DFT/B3LYP/6-31+G(d,p) methods, including NBO charges. The concept of charge on an atom is theoretically indeterminate, and only charges obtained by calculations carried out by one method can be discussed. It is known that Mulliken charges do not reflect the real distribution of electric charge between atoms and are rather sensitive to the choice of the basis set. However, they are convenient for a qualitative assessment of the charge distribution, comparison of their values during structure rearrangement, and determination of electrophilic and nucleophilic centers of possible attacks; therefore, they are currently used to analyze the electronic properties of molecules in most studies in solving such problems. The Mulliken charges in the DFT calculation have more negative values on the nitrogen atoms N_{19}, N_{20} and the oxygen atom O_{24}, but the charges on the carbon atoms H_{26} and H_7 are more positive. The charge calculated by the NBO method shows a negative value on the C_1 atom, which contributes to the formation of another $C_1H_7\ldots N_{20}$ hydrogen bond with a length of 2.517Å and an angle $C_1H_7\ldots N_{20}$ has a value of 93.886^0.

Table 4. Selected Mulliken charges for the Hydrazo-III tautomer, according to the PM3 method and Mulliken and NBO charges according to the DFT/B3LYP/6-31+G(d,p) method.

Atom	PM3	DFT	
	Mulliken	Mulliken	NBO
N_{19}	0.124	-0.140523	-0.39060
N_{20}	-0.013	-0.246423	-0.19872
C_{21}	-0.278	0.058171	0.01393
C_{22}	0.339	0.662464	0.52630
O_{24}	-0.343	-0.450326	-0.58773
H_{26}	0.129	0.397258	0.47082
C_1	0.054	0.749647	-0.21562
H_7	0.157	0.196762	0.30187
C_5	0.283	0.111818	0.35912
C_6	-0.165	-0.576378	0.11936
O_{17}	-0.256	-0.493252	-0.69236
C_4	-0.715	-0.565576	-0.39935
S_{12}	2.423	1.890234	2.38307
O_{13}	-0.896	-0.546063	-0.93590
H_{18}	0.281	0.448692	0.55076

To study the intramolecular interactions that promote the formation of hydrogen bonds, we analyzed the natural bond orbitals (NBO). The Gaussian program contains version 3.1 of the NBO program. The NBO method encompasses a set of algorithms that extract fundamental bond concepts from Hartree-Fock (HF) and density functional theory (DFT) calculations and illustrate the deciphering of the molecular wave function in terms well understood by chemists: Lewis structures, charge, bond order, bond type, hybridization, resonance, donor-acceptor interactions, etc. (Glendening *et al.,* 2012). In NBO analysis, the initial basis set of atomic orbitals is transformed into natural bond orbitals (NBO) corresponding to the Lewis chemical picture and all possible interactions between donor-occupied Lewis-type NBO orbitals (bond or lone pair) and formally unoccupied acceptor orbitals (antibonding or Rydberg) non-Lewis NBO orbitals are studied. The delocalization of the electron density between these orbitals corresponds to a stabilizing donor-acceptor interaction. Natural orbitals are described in great detail in (Weinhold *et al.,* 2005). The NBO method provides information about the interaction in both filled and virtual orbitals. In the analysis of the second-order perturbation theory of the Fock matrix in the NBO basis, estimates of the second-order perturbation energy E(2) of donor-acceptor interactions with charge transfer are summarized. The significant delocalization effects are determined (Reed *et al.,* 1988). As a stabilizing factor, the delocalization of the electron density leads to an energy gain. For each NBO donor (i) and NBO acceptor (j), the energy stabilizing the donor-acceptor interaction E(2) associated with electron density delocalization is estimated using the second-order perturbation theory:

$$E(2) = \Delta E_{ij} = q_i \frac{F(i,j)^2}{\varepsilon_j - \varepsilon_i},$$

where q_i is the population of the donor orbital, ε_i and ε_j are the diagonal elements of the Fock matrix corresponding to the orbital energy of the donor and acceptor NBO orbitals, respectively, F (i, j) are the off-diagonal elements of the Fock NBO matrix. The NBO analysis allowed us to find out which orbital interactions are mainly involved in the

stability of Hydrazo-III. Table 5 lists selected donor-acceptor interactions for the Hydrazo-III tautomer.

Table 5. Selected perturbation energies of the second order of the Fock matrix and the population of the Hydrazo-III molecule in the gas phase according to the results of calculations by the DFT/B3LYP/6-31+G(d,p) method

Donor (i)	Type	ED (i)	Acceptor (j)	Type	ED (j)	E (2)	E(j)-E(i)	F(i,j)
O_{24}	n (2)	1.88484	N_{19}-H_{26}	σ*	0.06199	13.12	0.71	0.087
O_{24}	n (1)	1.96696	N_{19}-H_{26}	σ*	0.06199	5.47	1.11	0.070
O_{24}	n (2)	1.88484	H_{26}	RY*(1)	0.00309	0.66	1.29	0.027
C_{22}-O_{24}	σ	1.99548	N_{19}-H_{26}	σ*	0.06199	0.65	1.48	0.028
O_{13}	n (2)	1.81591	O_{17}-H_{18}	σ*	0.04330	10.12	0.77	0.082
O_{13}	n (1)	1.97239	O_{17}-H_{18}	σ*	0.04330	5.70	1.25	0.076
O_{13}	n (3)	1.78264	O_{17}-H_{18}	σ*	0.04330	3.77	0.76	0.050
S_{12}-O_{13}	σ*	0.15857	O_{17}-H_{18}	σ*	0.04330	0.54	0.19	0.029
O_{17}	n (1)	1.96681	N_{19}-H_{26}	σ*	0.06199	1.96	1.01	0.040
O_{17}	n (2)	1.82218	C_5	n (1)	0.93939	66.67	0.19	0.127
N_{20}	n (1)	1.92868	C_1-H_7	σ*	0.01530	0.72	0.86	0.023
N_{20}	n (1)	1.92868	N_{19}-H_{26}	σ*	0.06199	9.00	0.81	0.077
C_3-C_4	π*	0.42754	C_1-C_2	π*	0.41678	233.67	0.02	0.087
C_5	n (1)	0.93939	C_6-N_{19}	π*	0.83255	186.51	0.09	0.122
C_5	n (1)	0.93939	C_3-C_4	π*	0.42754	59.21	0.14	0.098
O_{10}	n (3)	1.45220	N_9-O_{11}	π*	0.62856	161.31	0.14	0.137
C_6-N_{19}	π*	0.83255	C_1-C_2	π*	0.41678	126.27	0.07	0.103
C_6-N_{19}	π*	0.42754	N_{20}-C_{21}	π*	0.28959	27.94	0.06	0.049
C_6-N_{19}	π	1.78500	N_{20}-C_{21}	π*	0.28959	27.47	0.34	0.088
C_1-C_2	π	1.63918	C_6-N_{19}	π*	0.83255	30.02	0.22	0.082
C_1-C_2	π	1.63918	N_9-O_{11}	π*	0.62856	24.88	0.15	0.058
C_1-C_2	π	1.63918	C_3-C_4	π*	0.42754	26.54	0.27	0.076
C_3-C_4	π	1.71103	C_5	n (1)	0.93939	55.46	0.14	0.097
S_{12}-O_{13}	σ*	0.15857	S_{12}-O_{14}	σ*	0.14589	69.08	0.02	0.074
N_{28}	n (1)	1.64980	C_{23}-O_{25}	π*	0.31633	49.93	0.31	0.112

The NBO analysis confirmed that hyperconjugation interaction is the main reason for the greater stability of the Hidrazo-III tautomer. During donor-acceptor interaction, interactions with charge transfer from donors-lone pairs of oxygen and nitrogen to loosening π* and σ* orbitals of the nearest bonds are observed: n → σ* and n → π*. The strongest hyper conjugated interaction with a stabilization energy of 233.67 kcal/mol is associated with the delocalization of the electron density inside the benzene ring, corresponds to the redistribution of charges between the loosening π* orbitals of the bonds of the benzene ring with charge transfer from the C_3-C_4 donor to the C_1C_2 acceptor.

The energies of 186.51 and 59.21 kcal/mol correspond to the charge transfer from the lone pair of electrons of the C_5 atom of the benzene ring to the loosening π* orbitals of the C_6N_{19} and C_3-C_4 $n_{C5} \rightarrow \pi^*_{C6\text{-}N11}$ / $\pi^*_{C3\text{-}C4}$ bonds. The energy of 161.31 kcal/mol corresponds to the charge transfer from the donor lone pair of the O_{10} oxygen atom to the loosening π* acceptor orbital of the N_9O_{11} $n \rightarrow \pi^*_{N9\text{-}O11}$ bond. The formation of the resonant hydrogen bond $N_{19}H_{26}…O_{24}$ is confirmed by a strong donor-acceptor interaction with charge transfer from the lone pairs of the O_{24} oxygen atom to the anti-bonding σ^*orbital of the $N_{19}H_{26}$ bond: $n(1)_{O_{24}} \rightarrow \sigma^*_{N_{19}-H_{26}}$ and $n(2)_{O_{24}} \rightarrow \sigma^*_{N_{19}-H_{26}}$ with a delocalization energy of 13.12 and 5.47 kcal/mol, respectively, and from the lone oxygen pair O_{24} to the anti-bonding Rydberg orbital of the H_{26} atom with an energy of 0.66 kcal/mol. Inside the resonance ring, electron density delocalization is observed from the σ orbial of the $C_{22}O_{24}$ bond to the anti-bonding σ^* orbital of the $N_{19}H_{26}$ $\sigma_{C_{22}-O_{24}} \rightarrow \sigma^*_{N_{19}-H_{26}}$bond with a stabilization energy of 0.65 kcal/mol.

Another strong hydrogen bond $O_{17}H_{18}…O_{13}$ is confirmed by charge transfer from lone pairs of the O_{13} oxygen atom, as well as from the anti-bonding $S_{12}O_{13}$ orbital of the formed ring to the anti-bonding σ^* orbital of the $O_{17}H_{18}$ bond with $n(2)_{O_{13}}/n(1)_{O_{13}}/ n(3)_{O_{13}} \rightarrow \sigma^*_{O_{17}-H_{18}}$ having energies of 10.12, 5.70, 3.77 and 0.54 kcal/mol, respectively.

The weak hydrogen bond $N_{19}H_{26}…O_{17}$, which completes the formation of a three-centered hydrogen bond, was confirmed by charge transfer from the lone pair of the O_{17} oxygen atom to the anti-bonding σ^* orbital of the $N_{19}H_{26}$ bond with stabilization energy of 1.96 kcal/mol. A fairly strong interaction with a delocalization energy of 66.67 kcal/mol with charge transfer from the lone pair of the strongly negative O_{17} oxygen atom (-0.692) is transferred to the lone pair of the C_5 atom (0.359) of the benzene ring.

Analysis of NBO indicates the formation in the Hydrazo-III tautomer of another weak hydrogen bond $C_1H_7…N_{20}$ with an interaction energy of 0.72 kcal/mol and charge transfer $n(1)_{N_{20}} \rightarrow \sigma^*_{C_1-H_7}$ form the lone pair of the nitrogen atom N_{20} to the anti-bonding σ^* orbital C_1H_7 bond. The lone pair of electrons of the nitrogen atom N_{20} also transfers a charge to the anti-bonding σ^* orbital $N_{19}H_{26}$ bond with a destabilization energy of 9.00 kcal/mol.

Interactions between the anti-bonding π^* orbitals of the C_6-N_{19} donor bonds and the C_1-C_2 and N_{20}-C_{21} acceptors $\pi^*_{C_6-N_{19}} \rightarrow \pi^*_{C_1-C_2}/\pi^*_{N_{20}-C_{21}}$ are accompanied by a stabilization energy of 126.27 and 27.94 kcal/mol, respectively. The bonding π orbital of the C_6-N_{19} bond interacts with the loosening orbital π^* of the $N_{20}-C_{21}$ bond: $\pi_{C_6-N_{11}} \rightarrow \pi^*_{N_{20}-C_{21}}$ with conjugation energy of 27.47 kcal/mol.

The C_1-C_2 and C_3-C_4 bonding π orbitals of the benzene ring are donors for the acceptor π^* orbitals of the C_6-N_{19}, N_9-O_{11}, C_3-C_4 bonds and the C_5 lone pair with stabilization energies of 30.02 and 55.46 kcal/mol, respectively: $\pi_{C_1-C_2} \rightarrow \pi^*_{C_6-N_{19}}/ \pi^*_{N_9-O_{11}}/\pi^*_{C_3-C_4}$ and $\pi_{C_3-C_4} \rightarrow n(1)_{C_5}$. Note that interactions of the $\pi \rightarrow \pi^*$ type with charge transfer are formed due to the overlap of bonding and anti-bonding π orbitals, which are responsible for the conjugation of the corresponding π bonds, and lead to the stabilization of the system. The loosening σ^* orbitals of neighboring S=O bonds of the sulfo group interact with each other $\sigma^*_{S_{12}-O_{13}} \rightarrow \sigma^*_{S_{12}-O_{14}}$ with a stabilization energy of 69.08 kcal/mol. A strong interaction with an energy of 49.93 kcal/mol is observed during the transfer of an electron cloud from the nitrogen lone pair donor N_{28} to the acceptor anti-bonding π^* orbital of the $C_{23}O_{25}$ bond in the β −diketone fragment. In the work, visual three-dimensional pictures of the HOMO - LUMO orbitals of the Hydrazo-III

tautomer were obtained using the GaussView visualizer program (Fig.4). Fig.4 also shows the energies of the HOMO - LUMO orbitals and the energy gap for the Hydrazo-III tautomer. Red colour corresponds to a negative charge (the presence of electrons), and green to a positive charge (the absence of electrons). Analysing the visual image of HOMO-LUMO orbitals, one can determine which atoms and bonds of these orbitals the electron density is concentrated and the areas where electronic transitions occurred between these orbitals. Analysis showed that in the HOMO orbital, the electron density is located on the O_{25} and O_{24} oxygen atoms of the β-diketone fragment and covers the C_{23}-C_{21}, C_{21}-C_{22}, and C_{21} -N_{20} bonds. On the HOMO orbital of the benzene ring, the electron density embraces the bonds with the C_1, C_6, C_5 and, C2, C3 atoms and is located on the oxygen atom O_{17} of the hydroxyl group of the substituent in the benzene ring.

Upon transition to the LUMO orbital, the electron density shifts to the nitro group of the substituent of the benzene ring, covering the atoms and bonds of $C_2N_9O_{10}O_{11}$, completely freeing the β-diketone fragment and the hydrazo group, as well as the C_6 and C_4 atoms in the Hydrazo-III benzene ring from electron density.

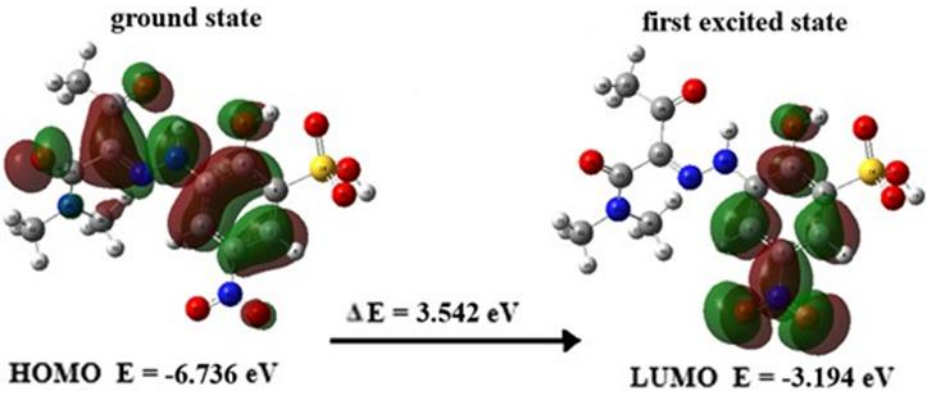

Fig. 4. HOMO and LUMO and their difference for Hydrazo-III tautomer (DFT/B3LYP/6−31+G(d,p))

Three-dimensional surfaces of the molecular electrostatic potential MEP are considered to be the most informative for determining the reactivity of a molecule. The molecular electrostatic potential V(r) is created by a system of nuclei and electrons, formulated directly from Coulomb's law and is a fundamental property of the system. When evaluated in the outer regions of a molecule, it shows how the molecule "feels" like an approaching reactant, and therefore plays a key role in explaining the reactivity of the molecule, especially for non-covalent interactions. The molecular electrostatic potential of a molecule is expressed by the following equation (Murray & Politzer, 2011):

$$V(r) = \sum_A \frac{Z_A}{|R_A - r|} - \int \frac{\rho(r')dr'}{|r' - r|}$$

where Z_A is the charge on the nucleus A located at point R_A, and $\rho(r')$ is the electron density. The first term in the expression is the effect of the nuclei, and the second is the effect of the electrons. These two terms have opposite signs and therefore opposite effects. V(r) is their resultant at each point *r*, is an indicator of the total electrostatic effect created at point *r* by the total distribution of the total charge (electrons + nuclei) of the molecule.

Initially, a computer program calculates a large number of electrostatic potential energies at a given distance from the nuclei of the molecule. Next, the program superimposes the calculated data on the electron density model of the molecule obtained from the Schrödinger equation. MEP surfaces visualize the 3D total charge distribution (electrons + nuclei) within a molecule, visually demonstrating the differently charged regions of the molecule, thus displaying the most likely areas for electrophilic/nucleophilic attack by charged reactants. Different electrostatic potential values on the surface are shown in different colors. Red and yellow colors are areas with a low, negative electrostatic potential, characterized by an abundance of electrons, subject to electrophilic attack, proton attraction. Blue color - an area with high positive potential, a relative absence of electrons, corresponds to the repulsion of a proton - this is the area of nucleophilic attack. The green color corresponds to zero potential. The potential increases in the order red < orange < yellow < green < blue. The MEP maps of the Hydrazo-III tautomer calculated by the DFT/B3LYP/6-31+G(d,p) method in gaseous and aqueous media are presented in Fig.5. The color code of the MEP map ranges from $-8.858e^{-2}$ a.u. (most saturated red) to $+8.858e^{-2}$(most saturated blue). Regions of negative electrostatic potential are usually associated with a lone pair of electronegative oxygen atoms.

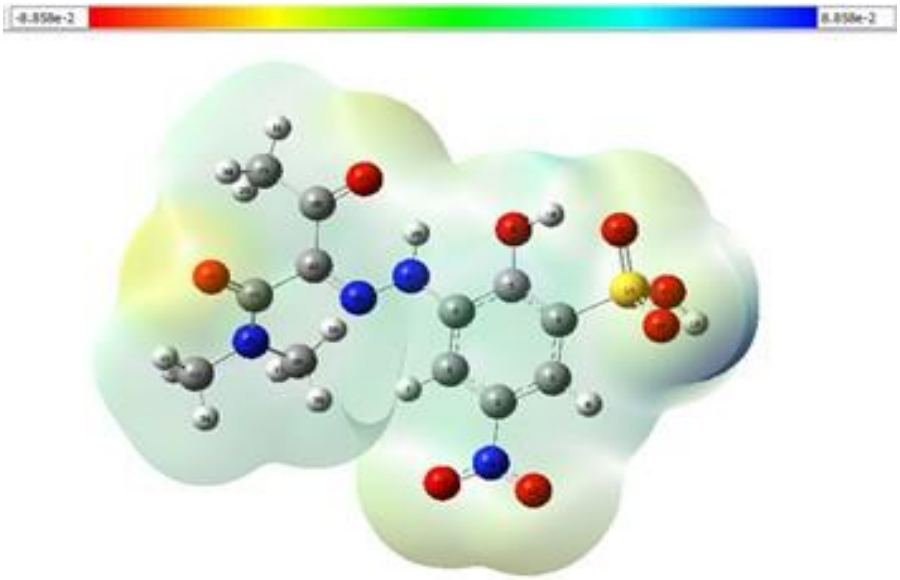

Figure 5. MEP map for Hydrazo-III tautomer according to the DFT/B3LYP/6−31+G(d,p) method

As can be seen from the MEP map, the most active centers of the alleged attacks and places for the proposed complex formation is the O_{25} oxygen atom of *β*-diketone, where a bright yellow color is observed, indicating that in this configuration this oxygen atom does not have intramolecular interactions and is ready for the proposed complexation. Thus, the oxygen atom O_{25} will act as a nucleophile due to the presence of a lone pair of electrons. The blue color is observed above the H_{16} hydrogen atom of the SO_3H sulfo group. Hydrogen bonds $N_{19}H_{26}$ …O_{24}, $N_{19}H_{26}$ …O_{17}, $O_{17}H_{18}$ …O_{13}, and C_1H_7…N_{20} already formed in this tautomer remove the color between these atoms, indicating the alignment of electrostatic potentials responsible for intramolecular hydrogen bonds. Thus, the oxygen atom O_{25} is the most reactive for the electrophilic

attack, and the hydrogen atom H_{16} will be the center of a possible nucleophilic attack. Thus, the electrostatic potential plays a key role in explaining the reactivity of the Hydrazo-III tautomer.

4. Conclusion

The spatial and electronic structures of eight tautomers of β-diketones were studied and analyzed using PM3 and DFT quantum chemistry methods. It is found that all tautomers have a planar structure. According to the results of both calculation methods, the Hydrazo-III tautomer has the most stable and compact structure. The NBO analysis revealed areas with delocalization of electron density, providing information on possible charge transfer pathways in the studied compounds. NBO analysis allowed us to determine which intramolecular and orbital interactions are involved in the stabilization of Hydrazo-III and the formation of a strong hydrogen bond in this tautomer. Such hydrogen bonding promotes the formation of the RAHB resonance ring on the side of the weak substituent in the β-diketone, which confirms the data from the calculation of the geometry and charge distribution on the atoms. The MEP maps allowed us to determine the sites of possible electrophilic and nucleophilic attacks in Hydrazo-III. The most active centers of putative attacks and sites of putative complexation are the oxygen atom O25 of β-diketone, which has no intramolecular interactions and is ready for putative complexation. HOMO-LUMO analysis of orbital energies allowed us to calculate global reactivity descriptors, which showed that the Hydrazo-III tautomer has the greatest reactivity. Our results may be useful to experimentalists dealing with the reactivity problems of this class of compounds.

References

Bertolasi, V., Gilli, P., Ferretti, V., Gilli, G. & Vaughan, K. (1999). Interplay between steric and electronic factors in determining the strength of intramolecular resonance-assisted NH···O hydrogen bond in a series of *β*-ketoarylhydrazones. *New Journal of Chemistry*, *23*(12), 1261-1267.

Blatov, V.A., Shevchenko, A.P. & Peresypkina, E.V. (2005). *Semiempirical Computational Methods of Quantum Chemistry: A Textbook*. Publishing House Univer-Groupp, Samara.

Dennington, R., Keith, T.A. & Millam, J.M. (2016). *GaussView, version 6.0. 16.* Semichem Inc Shawnee Mission KS.

Frisch, M.J., Trucks, G.W., Schlegel, H.B., Scuseria, G.E., Robb, M.A., Cheeseman, J.R. & Pople, J.A. (2013). *Gaussian 03, revision c. 02*; Gaussian, inc.: Wallingford, ct, 4.

Gilli, P., Bertolasi, V., Ferretti, V. & Gilli, G. (2000). Evidence for intramolecular N− H···O resonance-assisted hydrogen bonding in β-enaminones and related heterodienes. A combined crystal-structural, IR and NMR spectroscopic and quantum-mechanical investigation. *Journal of the American Chemical Society*, *122*(42), 10405-10417.

Gilli, P., Bertolasi, V., Pretto, L., Lyčka, A. & Gilli, G. (2002). The nature of solid-state N− H···O/O−H··· N tautomeric competition in resonant systems. Intramolecular proton transfer in low-barrier hydrogen bonds formed by the ···OC− CN− NH···⇄··· HO− CC− NN··· Ketohydrazone− Azoenol System. A variable-temperature x-ray crystallographic and DFT computational study. *Journal of the American Chemical Society*, *124*(45), 13554-13567.

Gilli, P., Pretto, L., Bertolasi, V. & Gilli, G. (2009). Predicting hydrogen-bond strengths from acid− base molecular properties. The p K a slide rule: Toward the solution of a long-lasting problem. *Accounts of Chemical Research*, *42*(1), 33-44.

Glendening, E.D., Landis, C.R. & Weinhold, F. (2012). Natural bond orbital methods. *Wiley Interdisciplinary Reviews: Computational Molecular Science*, *2*(1), 1-42.

Gurbanov, A.V., Kuznetsov, M.L., Demukhamedova, S.D., Alieva, I.N., Godjaev, N.M., Zubkov, F.I. & Pombeiro, A.J. (2020). Role of substituents on resonance assisted hydrogen bonding vs. intermolecular hydrogen bonding. *CrystEngComm*, *22*(4), 628-633.

Hansen, P.E. (2016). Methods to distinguish tautomeric cases from static ones. *Tautomerism: Ideas, Compounds, Applications*, 35-74. Weinheim, Germany.

Hansen, P.E. (2021). A spectroscopic overview of intramolecular hydrogen bonds of NH···O, S, N type. *Molecules, 26(*9), 2409-2431.

Hansen, P.E., Spanget-Larsen, J. (2017). NMR and IR investigations of strong intramolecular hydrogen bonds. *Molecules, 22*(4), 552-572.

Jezierska, A., Tolstoy, P.M., Panek, J.J. & Filarowski, A. (2019). Intramolecular hydrogen bonds in selected aromatic compounds: Recent developments. *Catalysts, 9*(11), 909-928.

Koopmans, T. (1934). Uber die zuordnung von wellenfunktionen und eigenwerten zu den einzelnen elektronen eines atoms. *Physica, 1(*1-6), 104-113.

Kopylovich, M.N., Mahmudov, K.T., & Pombeiro, A.J.L. (2011). Poly(vinil) chloride membrane copper-selective electrode based on 1-phenyl-2-(2-hydroxyphenylhydrazo)butan-1,3-dione. *J. Hazard. Mater.*, *186* (2-3), 1154-1162.

Kopylovich, M.N., Mahmudov, K.T., Guedes da Silva, M.F.C., et al. (2011). Ortho-hydroxyphenylhydrazo-*β*-diketones: tautomery, coordination ability, and catalytic activity of their copper(II). Complexes toward oxidation of cyclohexane and benzylic alcohols. *Inorg.Chem.*, *50*(3), 918-931.

Kuznik, W., Kityk, I. V., Kopylovich, M. N., Mahmudov, K. T., Ozga, K., Lakshminarayana, G., & Pombeiro, A. J. L. (2011). Quantum chemical simulations of solvent influence on UV–vis spectra and orbital shapes of azoderivatives of diphenylpropane-1, 3-dione. *Spectrochimica Acta Part A: Molecular and Biomolecular Spectroscopy*, *78*(4), 1287-1294.

Ma, Z., Mahmudov, K. T., Aliyeva, V. A., Gurbanov, A. V., da Silva, M. F. C. G., & Pombeiro, A. J. (2021). Peroxides in metal complex catalysis. *Coordination Chemistry Reviews*, *437*, 213859.

Mahmudov, K. T., Maharramov, A. M., Aliyeva, R. A., Aliyev, I. A., Kopylovich, M. N., & Pombeiro, A. J. (2010). Ion pairs of 5, 5-dimethyl-2-(2-hydroxy-3, 5-disulfophenylhydrazo) cyclohexane-1, 3-dione with cationic surface-active substances as analytical reagent for determination of copper (II). *Analytical Letters*, *43*(18), 2923-2938.

Mahmudov, K.T. Aliyeva, R.A., Gadjieva, S.R., & Chyragov, F.M. (2008). Photometric determination of copper (II) in nickel alloys using azoderivatives of ethylacetoacetate. *J. Analyt. Chem.*, *63*(5), 435-438.

Mahmudov, K.T., Kopylovich, M.N., & Pombeiro, A.J.L. (2013). Coordination chemistry of arylhydrazones of methylene active compounds. *Coord. Chem. Rev.*, *257*, 1244-1281.

Martinez, R.F., Matamoros, E., Cintas, P., &Palacios, J.C. (2020). Imine or Enamine? Insights and predictive guidelines from the electronic effect of substituents in H-bonded salicylimines. *J. Org. Chem.*, *85*(9), 5838-5862.

Maspero, A., Nardo, L., & Palmisano, G. (2022). *Pharmaceuticals*, Special Issue *β*-Diketones and Their Derivatives: Synthesis, Characterization and Biomedical Applications, February.

Murray, J.S., Politzer, P. (2011). The electrostatic potential: An overview. *Wiley Interdisciplinary Reviews: Computational Molecular Science*, *1*(2), 153-163.

Reed, A.E., Curtiss, L.A., & Weinhold, F. (1988). Intermolecular interactions from a natural bond orbital, donor-acceptor viewpoint. *Chemical Review*, 88, 899-926.

Shchegol'kov, E.V., Burgart, Y.V., Khudina, O.G., Saloutin, V.I., & Chupakhin, O.N. (2010). 2-(Het)arylhydrazono-1,3-dicarbonylcompounds in organic synthesis. *Rus. Chem. Rev.*, *79*(1), 31-61.

Sobczyk, L., Chudoba, D., Tolstoy, P.M., & Filarowski, A. (2016). Some brief notes on theoretical and experimental investigations of intramolecular hydrogen bonding. *Molecules*, *21*(12), 1657-1675.

Udagawa, T., Murphy, R. B., Darwish, T. A., Tachikawa, M., & Mori, S. (2021). H/D Isotope Effects in Keto-Enol Tautomerism of β-Dicarbonyl Compounds—Importance of Nuclear Quantum Effects of Hydrogen Nuclei—. *Bulletin of the Chemical Society of Japan*, *94*(7), 1954-1962.

Viswanathan, A., Kute, D., Musa, A., Mani, S. K., Sipilä, V., Emmert-Streib, F., ... & Kandhavelu, M. (2019). 2-(2-(2, 4-dioxopentan-3-ylidene) hydrazineyl) benzonitrile as novel inhibitor of receptor tyrosine kinase and PI3K/AKT/mTOR signaling pathway in glioblastoma. *European Journal of Medicinal Chemistry*, *166*, 291-303.

Weinhold, F., Landis, C.R. (2005). *Valency and bonding: a natural bond orbital donor-acceptor perspective*. Cambridge University Press.